



## Fabrication and characterization of solid oxide fuel cell cathodes made from nano-structured LSCF–SDC composite feedstock



J. Harris, C. Metcalfe, M. Marr, J. Kuhn, O. Kesler\*

Department of Mechanical & Industrial Engineering, University of Toronto, 5 King's College Road, Toronto, ON, Canada

### HIGHLIGHTS

- A plasma spray process was developed for a nano-structured LSCF–SDC feedstock.
- The effect of the cathode microstructure on the cell impedance was investigated.
- At higher temperatures, diffusion dominates the impedance of finely-mixed cathodes.
- Charge transfer kinetics affects the impedance of coarsely-mixed cathodes.
- At lower temperatures, impedances are more strongly affected by the TPB density.

### ARTICLE INFO

#### Article history:

Received 16 January 2013

Received in revised form

6 March 2013

Accepted 10 March 2013

Available online 29 March 2013

#### Keywords:

SOFC

Composite

Cathode

Plasma spray

LSCF

SDC

### ABSTRACT

Composite  $\text{La}_{0.6}\text{Sr}_{0.4}\text{Co}_{0.2}\text{Fe}_{0.8}\text{O}_{3-\delta}$  (LSCF) and  $\text{Ce}_{0.8}\text{Sm}_{0.2}\text{O}_{1.9}$  (SDC) cathodes for solid oxide fuel cells (SOFCs) were fabricated by axial-injection plasma spraying. Fine mixing of the ceramic phases was achieved by using a nano-structured feedstock that contained both phases agglomerated together in larger particles. Preliminary investigations explored the effects of varying the process parameters, and cathodes were characterized by XRD and SEM. Metal-supported symmetrical cells were made with several promising sets of process parameters, and the polarization resistance was measured from 550 °C to 750 °C. The cathode with the highest electrochemical performance was incorporated into a fuel cell with a yttria-stabilized zirconia (YSZ) electrolyte and a nickel–YSZ anode. A fuel cell with a coarsely-mixed composite cathode was also fabricated, and the effect of the cathode microstructure on cell impedance was studied using the analysis of differential impedance spectra.

© 2013 Elsevier B.V. All rights reserved.

### 1. Introduction

$\text{La}_{0.6}\text{Sr}_{0.4}\text{Co}_{0.2}\text{Fe}_{0.8}\text{O}_{3-\delta}$  (LSCF) is a common material for intermediate temperature (650 °C–750 °C) solid oxide fuel cell (SOFC) cathodes [1–4]. LSCF-containing cathodes have been shown to have higher electrochemical performance when they consist of a composite cathode with an ionic conductor such as gadolinia-doped ceria (GDC) or samaria-doped ceria (SDC) [1,4,5]. In general, a composite cathode with a fine microstructure is desirable to maximize performance: a cathode with a finer microstructure will have a greater triple phase boundary (TPB) density and therefore more electrochemical reaction sites.

Plasma spraying has emerged as a process for manufacturing planar metal-supported SOFCs [6–10]. Using this process, the fabrication of single-phase LSCF has been investigated in several studies [11–16]. Previously, we have fabricated composite LSCF–SDC cathodes by plasma spraying a feedstock that consisted of a heterogeneous mixture of LSCF powder and SDC powder [17–19]. These dry powders contained particles with large median diameters (between 30 and 40  $\mu\text{m}$ ) so that the material was flowable for plasma spraying. However, as a result of the large particle sizes, the LSCF and SDC phases were coarsely mixed in the cathodes.

The present article describes the development and characterization of composite cathodes in which the LSCF and SDC phases are more finely mixed. This fine mixing is attained by using a nano-structured composite plasma spray feedstock, in which each particle consists of an agglomerate of both LSCF and SDC phases.

\* Corresponding author. Tel.: +1 416 978 3835.

E-mail addresses: [jharris@mie.utoronto.ca](mailto:jharris@mie.utoronto.ca) (J. Harris), [kesler@mie.utoronto.ca](mailto:kesler@mie.utoronto.ca) (O. Kesler).

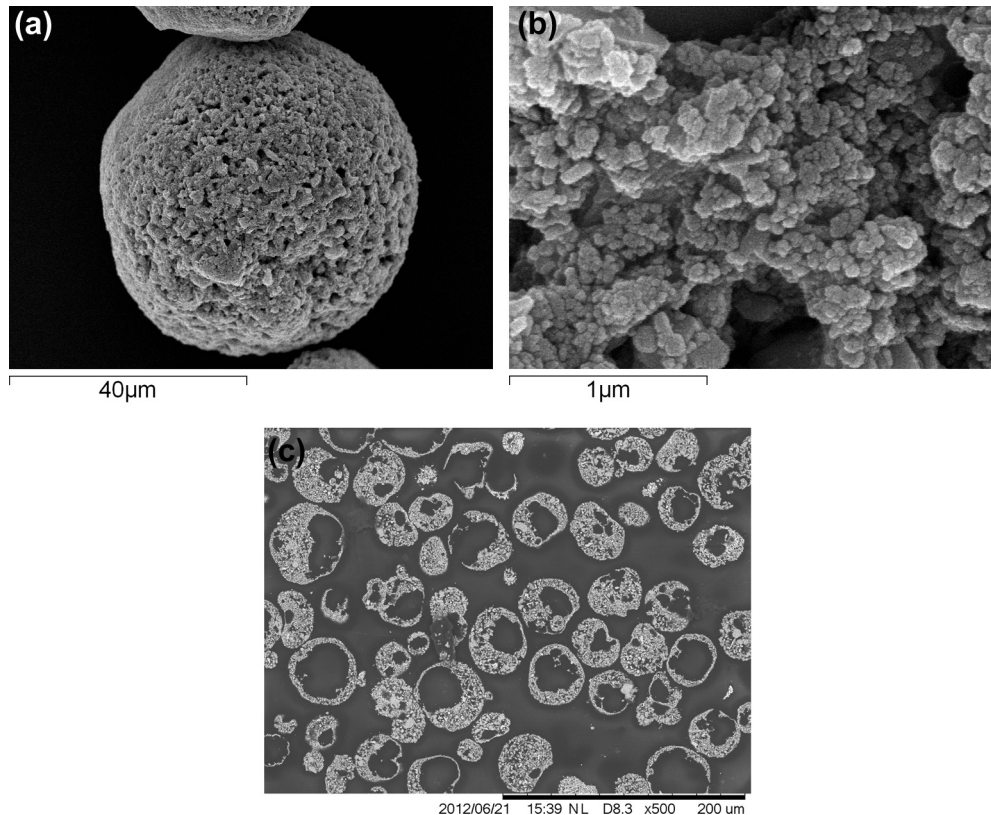


**Fig. 1.** Nano-structured composite LSCF–SDC agglomerates. Micrographs of (a) one particle, (b) the surface of one particle, (c) a polished cross-section of several particles.

## 2. Experimental method

### 2.1. Materials

Cathodes were fabricated from a nano-structured composite powder that consists of hollow spherical agglomerates composed of 60 wt% LSCF and 40 wt% SDC ( $\text{Ce}_{0.8}\text{Sm}_{0.2}\text{O}_{1.9}$ ). The commercial powder supplier (Inframet Advanced Materials, Manchester, CT, USA) formed the hollow agglomerates by spray drying a suspension of the two ceramic phases. Micrographs of these agglomerates are shown in Fig. 1. To improve the cohesion of the agglomerates, the as-received powder was heat treated for 5.5 h at a high temperature, ranging from 1025 to 1225 °C. Subsequently, the powder was separated by sieving into three size fractions: (−75 + 45) μm, (−45 + 32) μm, and −32 μm. Using laser light scattering, the  $d_{50}$  by volume of each size fraction was measured to be 59.7, 34.8, and 20.9 μm, respectively.

### 2.2. Cathode fabrication and process development

Cathodes were fabricated using axial-injection plasma spraying (Axial III Series 600, Northwest Mettech, North Vancouver, BC,

**Table 1**  
Range of Axial III torch parameters used for fabricating LSCF–SDC cathodes.

Parameter	Value
Plasma gas flow rate	200 slpm
Plasma gas composition	20–80% nitrogen, balance argon
Arc current	150 A per electrode pair (450 A total)
Nozzle size	9.52 and 12.7 mm
Standoff distance	75 mm

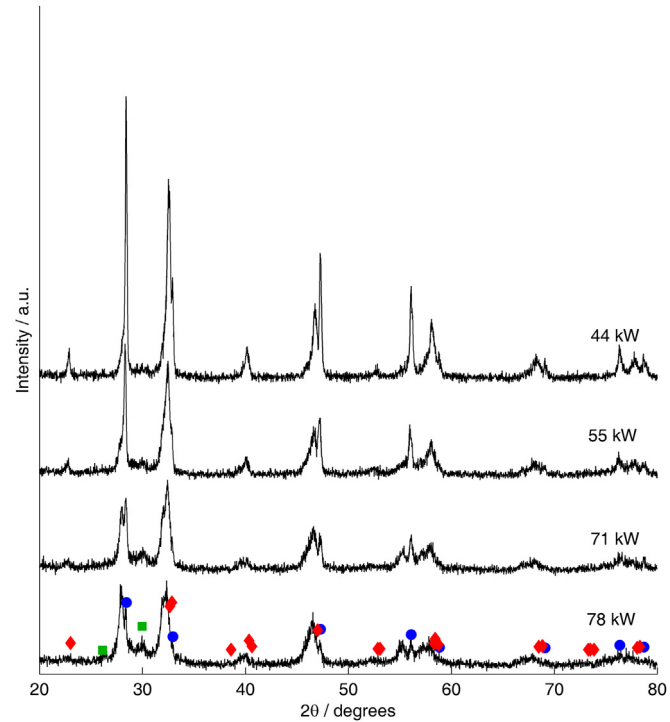


**Fig. 2.** X-ray diffraction patterns of LSCF–SDC cathodes produced with 44 kW, 55 kW, 71 kW, and 78 kW plasmas, corresponding to 20%, 40%, 60%, and 80% nitrogen plasma gas mixtures (balance argon). Reference peaks are shown for LSCF (♦), SDC (●), and  $\text{La}_2\text{O}_3$  (■).

**Table 2**

Deposition efficiency of plasma sprayed LSCF–SDC cathodes.

Plasma gas mixture	Plasma power	Deposition efficiency
80% N <sub>2</sub> /20% Ar	78 kW	81%
60% N <sub>2</sub> /40% Ar	71 kW	83%
40% N <sub>2</sub> /60% Ar	55 kW	81%
20% N <sub>2</sub> /80% Ar	44 kW	48%

Canada). With this plasma torch, feedstock powders were fed directly into the centre of the plasma and accelerated towards a substrate. The material partially melted in-flight, formed splats on porous 430 stainless steel substrates, and rapidly cooled to form cathode layers.

The range of processing parameters used to fabricate LSCF–SDC cathodes is summarized in Table 1. Initially, the effects of four process variables known to most significantly impact the properties of the plasma-sprayed cathode layers were investigated. These variables consisted of two plasma spray parameters (plasma gas composition and nozzle size) and two material attributes (size fraction of agglomerates and powder heat treating temperature). The plasma gas was composed of argon–nitrogen mixtures, and as the proportion of the gas mixture was changed, the power of the plasma varied. The size of the nozzle at the exit of the plasma torch affects the velocity of the plasma and the velocity of the particles during flight through the plasma. The size fraction of the agglomerates affects the extent to which the feedstock material melts during fabrication; it also affects the size and shape of the splats that make up the cathode microstructure. The last variable, the heat treating temperature, affects the cohesion of the agglomerates. It also affects the microstructure of the feedstock agglomerates: higher calcination temperatures cause the agglomerates to coarsen more than lower ones.

### 2.3. Characterization of cathode layers

To determine the range of process variables suitable for fabricating cathodes, the cathode phase compositions were evaluated

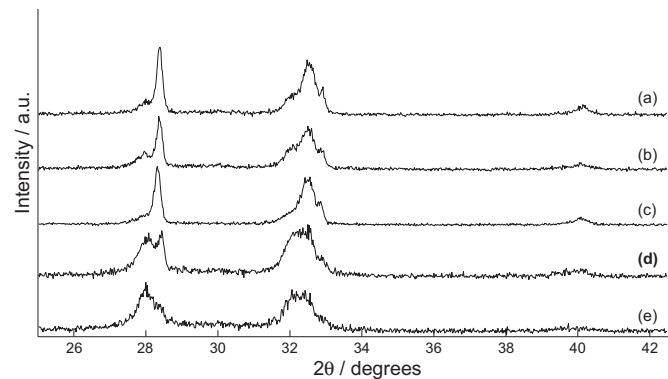


**Fig. 4.** X-ray diffraction patterns of LSCF–SDC cathodes produced using (a) 40% nitrogen/60% argon plasma gas mixture, 12.7 mm torch nozzle, and  $-75 + 45 \mu\text{m}$  feedstock particles, (b) 50% nitrogen/50% argon plasma gas mixture, 12.7 mm diameter torch nozzle, and  $(-75 + 45) \mu\text{m}$  feedstock particles, (c) 80% nitrogen/20% argon plasma gas mixture, 9.5 mm diameter torch nozzle, and  $(-45 + 32) \mu\text{m}$  feedstock particles, (d) 60% nitrogen/40% argon plasma gas mixture, 9.5 mm diameter torch nozzle, and  $(-45 + 32) \mu\text{m}$  feedstock particles, (e) 40% nitrogen/60% argon plasma gas mixture, 9.5 mm torch nozzle, and  $(-45 + 32) \mu\text{m}$  feedstock particles.

by X-ray diffraction (XRD) (Philips PW 1830 HT, PANalytical B.V., Almelo, Netherlands), and the microstructures were examined by scanning electron microscopy (SEM) (S590, S4500, and TM3000, Hitachi High-Tech, Tokyo, Japan). The surface roughnesses of cathodes were measured using an analog profilometer with a  $10 \mu\text{m}$  diamond stylus (Surfometer, Precision Devices Inc, Milan, MI, USA).

The gas transport properties of cathodes were evaluated in forced flow permeation tests, in which pressure differences were incrementally applied across cathodes on metal supports, and the mass flow rates of air were measured. Using Darcy's Law, the permeability ( $\kappa$ ) can be calculated using Equation (1), where  $Q$  is the mass flow rate,  $\Delta P/L$  is the pressure difference across a specimen of thickness  $L$ ,  $\mu$  is the kinematic viscosity of air, and  $A$  is the projected area across which the pressure is applied.

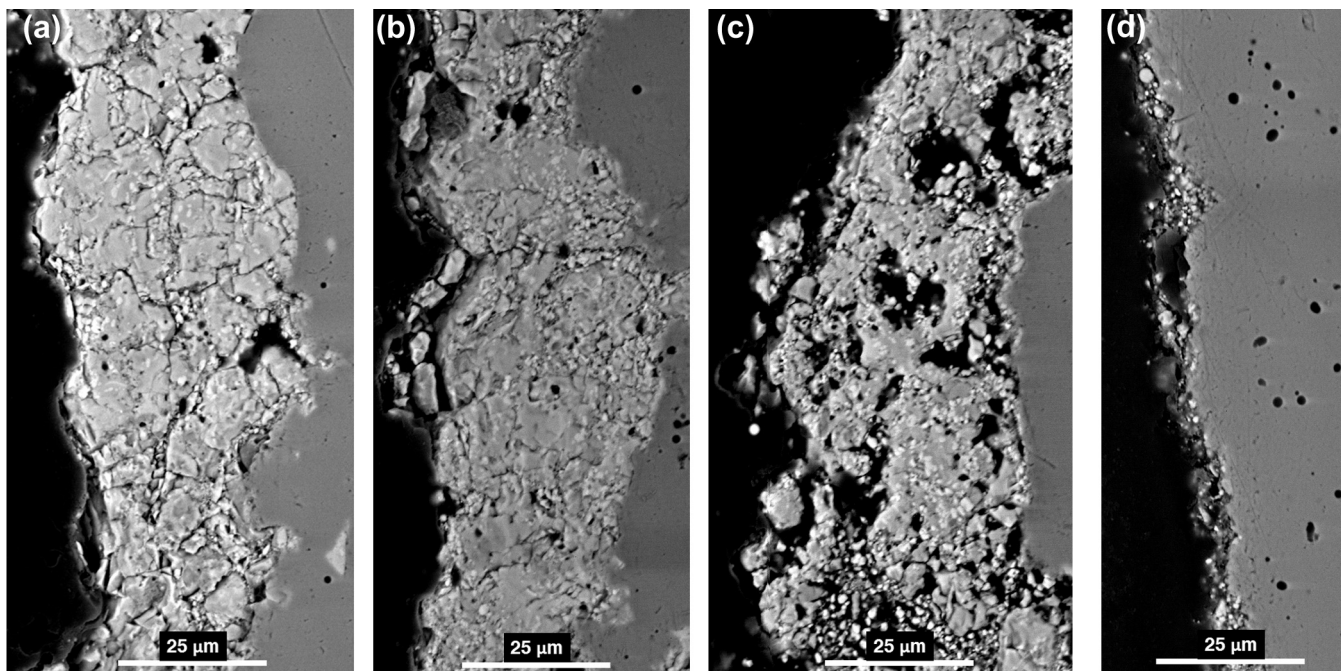


**Fig. 3.** Micrographs of cross sections of LSCF–SDC cathodes produced with (a) 80% nitrogen, (b) 60% nitrogen, (c) 40% nitrogen, (d) 20% nitrogen plasmas (balance argon).

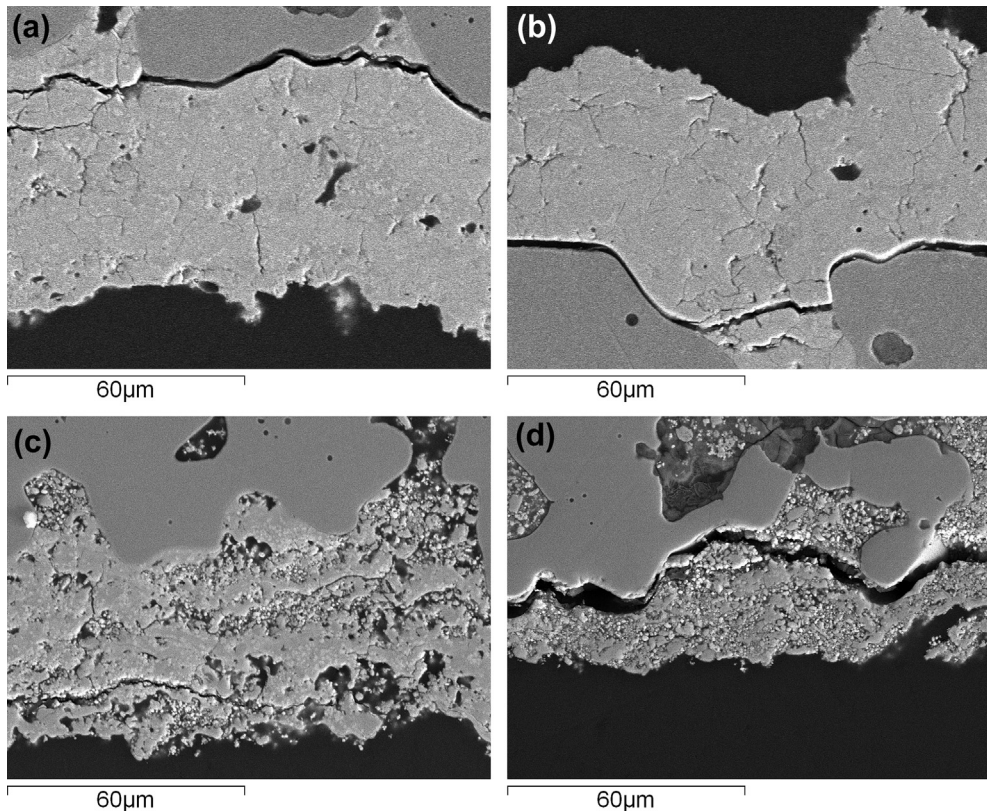


**Fig. 5.** Cross-sectional micrographs of LSCF–SDC cathodes (on metal supports) made with a smaller (9.5 mm) torch nozzle using plasma gases containing (a) 80% nitrogen, (b) 60% nitrogen, (c) 40% nitrogen, and (d) 20% nitrogen (balance of plasma gas is argon).

$$\kappa = \left( \frac{dQ}{d(\Delta P/L)} \right) \left( \frac{\mu}{A} \right) \quad (1)$$

#### 2.4. Electrochemical evaluation in symmetrical cells

Symmetrical button cells were fabricated on porous 430 stainless steel supports (Mott Corporation, Farmington, CT, USA) with a diameter of 25.4 mm. The cells have projected active areas of 1.00 cm<sup>2</sup> and consist of two cathodes separated by a YSZ electrolyte fabricated by suspension plasma spraying [20,21].

Tests were performed in test stations (FCSH-1000, Materials Mates Italia, Milano, Italy) with modified gas flow channels that distribute gases more evenly across the surfaces of the cell. On the metal support side of the cell, a coarse platinum mesh collected current by dry contact; on the electrode side of the cell, a layer of LSCF paste was stenciled on the cathode and contacted to a fine platinum wool current collector. Cells were initially heated to 750 °C and held at that temperature for 12 h prior to electrochemical testing. The total air flow rate used was 900 sccm. Using a four-wire configuration, electrochemical impedance spectroscopy was performed from 100 kHz to 10 mHz (SI 1470 and SI 1260, Solartron Analytical, Farnborough, UK) with a 10 mV amplitude, and the polarization resistances ( $R_p$ ) were calculated from the resulting impedance spectra.

#### 2.5. Fuel cell testing

Button fuel cells consisted of porous 430 stainless steel supports, nickel–YSZ anodes, YSZ electrolytes, and LSCF–SDC cathodes. These cells have the same dimensions as the symmetrical cells. The anode was fabricated by plasma spraying a powder feedstock as

previously reported [22] and the electrolyte was fabricated by suspension plasma spraying [21].

Fuel cell tests were performed in a custom-built apparatus. The fuel cell was clamped between two gold mesh current collectors with sufficient force so that contact pastes were not necessary. To keep anode and cathode gases separated, the cell was sealed with a compressed vermiculite gasket (Flexitallic LP, Deer Park, TX, U.S.A.) butted against the end of an alumina tube. Cells were initially heated to 750 °C with a 100% air atmosphere on the cathode side and 4% hydrogen/96% nitrogen on the anode side. Once heated, the anode gas composition was gradually increased to 100% hydrogen humidified at room temperature using a bubbler. The total gas flow rates were 1000 sccm and 200 sccm for the cathode and anode, respectively.

Electrochemical performance was measured using a four-wire configuration. Polarization curves were obtained from potentiodynamic tests from open circuit potential to 0.4 V (versus reference) at a rate of 5 mV min<sup>-1</sup>. Electrochemical impedance spectra were obtained by sweeping at 20 mV amplitude from 1 MHz to 10 mHz.

### 3. Results and discussion

#### 3.1. Effects of manufacturing process

##### 3.1.1. Effect of plasma gas composition

Preliminary cathode coatings were fabricated with argon–nitrogen plasmas with four different plasma gas compositions: 20%, 40%, 60%, and 80% nitrogen (balance argon) that resulted in powers of 44 kW, 55 kW, 71 kW, and 78 kW, respectively. A 12.7 mm plasma torch nozzle was used. The feedstock material was heat treated at 1125 °C and subsequently sieved between 45 μm (ASTM

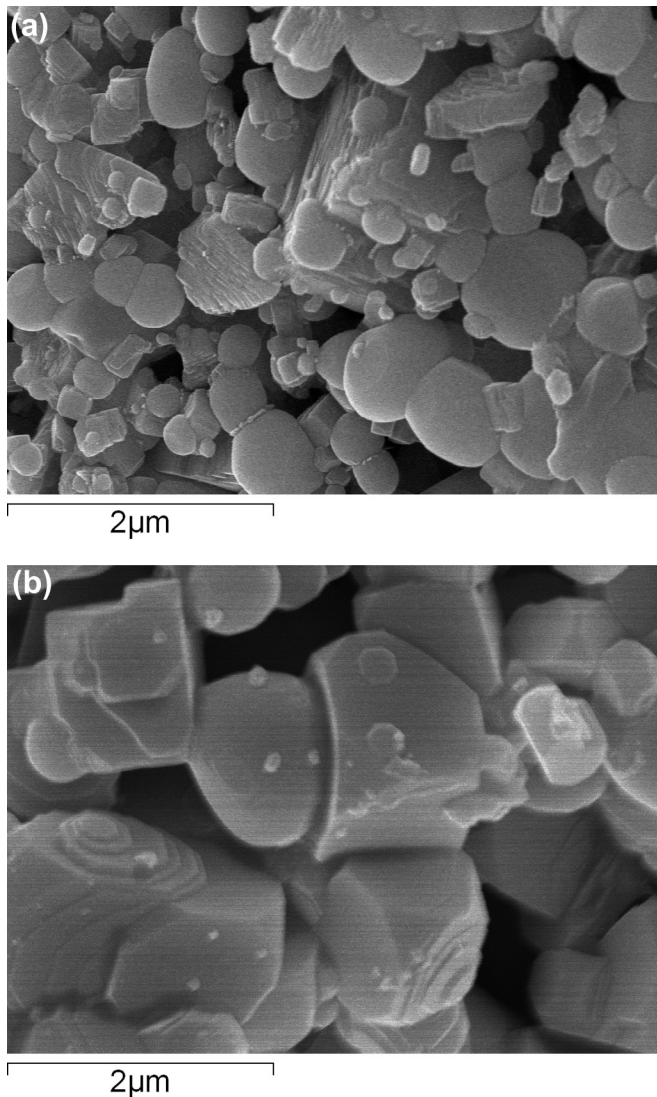


**Fig. 6.** Surface microstructure of an agglomerated LSCF–SDC particle that was heat treated at (a) 1125 °C, and (b) 1225 °C.

No. 325) and 32 μm (ASTM No. 450) meshes. Feedstock heat treated at 1025 °C disintegrated during feeding and therefore was not studied further. X-ray diffraction patterns of these cathodes, shown in Fig. 2, reveal partial decomposition of LSCF into La<sub>2</sub>O<sub>3</sub> (ICDD PDF 01-071-5408), which has a primary peak at  $2\theta = 30.0^\circ$ . Based on the intensity of this peak relative to the primary LSCF peak, LSCF decomposed less when lower plasma powers were used. This observation is consistent with several other studies [15,23,24] in which perovskite phases have decomposed when excessive powers were used during plasma spraying. Although the cathodes

produced with lower powers contain less decomposed LSCF, the cathode produced with a 20% nitrogen plasma is not viable because the process deposition efficiency was low (as listed in Table 2) and the cathode material adhered poorly to the metal support. Micrographs of these four cathode coatings are shown in Fig. 3: notably, the cathode produced with a 40% nitrogen plasma is the most porous of the cathodes produced with high deposition efficiencies.

To reduce the amount of lanthanum oxide in the cathodes, three process variables were modified separately: (1) a feedstock with larger particles was used, (2) a smaller torch nozzle was used, and (3) the powder feedstock was heat treated at a higher temperature.

### 3.1.2. Increasing the feedstock particle size

The feedstock with larger agglomerated particles consisted of material sieved between a 75 μm (ASTM No. 200) mesh and a 45 μm (ASTM No. 325) mesh. With this feedstock, cathodes were fabricated with 54 kW and 62 kW plasmas using 40% and 50% nitrogen plasmas, respectively. When the feedstock particles are larger, less surface area (relative to mass) is exposed directly to the plasma during fabrication. Compared to cathodes made from smaller feedstock particles, there was less decomposed material in the cathodes, as shown in the X-ray diffraction patterns in Fig. 4 (a) and (b). Traces of lanthanum oxide in the cathode appear to be low when both 40% and 50% nitrogen plasmas were used. However, when 40% nitrogen was used in the plasma, cathodes fabricated from the larger feedstock particles adhered poorly to the metal support: when we attempted to deposit an electrolyte on top of the cathode, the cathode material abraded, causing the electrolyte to delaminate. Therefore, a minimum plasma power of 62 kW (corresponding to a 50% nitrogen/50% argon plasma gas mixture) is necessary to fabricate cathodes from the (−75 + 45) μm powder.

### 3.1.3. Reducing the nozzle size

Cathodes fabricated with a smaller 9.52 mm diameter plasma torch nozzle also show less decomposed material in X-ray diffraction patterns, as shown in Fig. 4(c)–(e). It is believed that using the smaller nozzle kinetically limits decomposition because particle velocities are higher during plasma spraying, and thus the material is exposed to the plasma for a shorter time. As shown in the micrographs in Fig. 5, the cathodes were excessively dense when plasmas containing 60% or more nitrogen were used. Additionally, cathodes made with a 20% nitrogen plasma had insufficient adhesion to the substrate: simply by hand, the cathode material could be easily wiped off the metal support.

### 3.1.4. Feedstock heat treating temperature

To investigate the effect of the heat treating temperature, the LSCF–SDC feedstock was heat treated for 5.5 h at a higher temperature, 1225 °C. Under this treatment, the particle microstructures coarsened significantly more than when the heat treating temperature was 1125 °C, as shown in Fig. 6. The coarser microstructure is less desirable than the fine microstructure: to maximize electrochemical performance, cathodes should have a fine

**Table 3**  
Process parameters used for fabricating symmetrical cells.

Cell	A	B	C	D
Feedstock	LSCF–SDC treated at 1125 °C and sieved (−45 + 32) μm	LSCF–SDC treated at 1125 °C and sieved (−45 + 32) μm	LSCF–SDC treated at 1125 °C and sieved (−75 + 45) μm	75 wt% (LSCF–SDC treated at 1125 °C and sieved −45 μm + 32 μm) 25 wt% starch
Plasma gas	200 slpm (40% N <sub>2</sub> /60% Ar)	200 slpm (40% N <sub>2</sub> /60% Ar)	200 slpm (50% N <sub>2</sub> /50% Ar)	200 slpm (40% N <sub>2</sub> /60% Ar)
Arc current	150 A per electrode pair (450 A total)	150 A per electrode pair (450 A total)	150 A per electrode pair (450 A total)	150 A per electrode pair (450 A total)
Nozzle diameter	12.7 mm	9.5 mm	12.7 mm	12.7 mm
Standoff distance	75 mm	75 mm	75 mm	75 mm

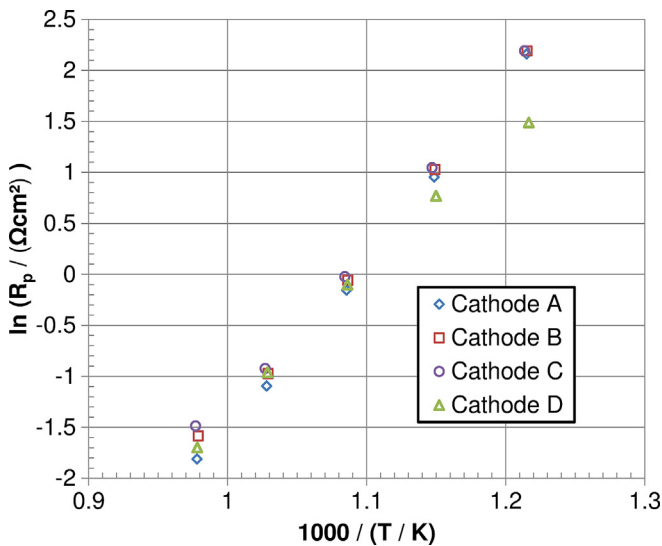


**Fig. 7.** Arrhenius plot of the symmetrical cell polarization resistances, measured from 550 °C to 750 °C.

microstructure with many electrochemical reaction sites. In general, much of the microstructure in the feedstock can be preserved in a plasma sprayed coating, so the feedstock treated at 1125 °C was thought to be more likely to result in a higher performing cathode. Cathodes were fabricated from a 1225 °C-treated feedstock using 55, 69, and 74 kW plasmas that were composed of 40, 50, and 60% nitrogen, respectively (balance argon). These cathodes deposited very poorly, resulting in thin layers, and none of these cathodes contained the desirable fine microstructure for an SOFC cathode.

Hence the feedstock treated at 1225 °C was not investigated further.

Ultimately, three sets of process parameters were selected for fabricated cathodes to be electrochemically tested. These cathodes adhered well to metal supports, had favourable microstructures (with high porosity and surface area), and showed minimal amounts of decomposed phases.

### 3.2. Symmetrical cell performance

Symmetrical cells were fabricated using three of the most promising sets of process parameters, listed as cathodes A, B, and C in Table 3. Additionally, a fourth symmetrical cell was made (cathode D) using the same process parameters as cathode A, except the feedstock was changed by mixing 25 wt% of starch with 75 wt% of the ceramic material.

The electrochemical impedance spectra were measured on symmetrical cells A, B, and C at 750 °C, 700 °C, 650 °C, 600 °C, and 550 °C, and the cell polarization resistances are plotted in an Arrhenius plot in Fig. 7. In this plot, the cells have polarization resistances that are very close to each other. At 650 °C, the cathode polarization resistances were 0.429, 0.472, and 0.489 Ω cm<sup>2</sup>/electrode for cells A, B, and C, respectively. The polarization resistances of these plasma sprayed symmetrical cells are within the range of polarization resistances of cathodes manufactured by traditional wet ceramic techniques [1,5]. At 650 °C, Murray et al. measured polarization resistances of LSCF–GDC cathodes ranging from approximately 0.1 Ω cm<sup>2</sup> to 0.6 Ω cm<sup>2</sup> [1]; similarly, Leng et al. measured polarization resistances of LSCF–GDC cathodes ranging from approximately 0.08 Ω cm<sup>2</sup> to 0.8 Ω cm<sup>2</sup> [5]. Both studies used a three-point setup to measure  $R_p$ , whereas in the present study, the symmetrical cell  $R_p$  was measured and contains contributions from two cathodes: one on each side of the electrolyte.

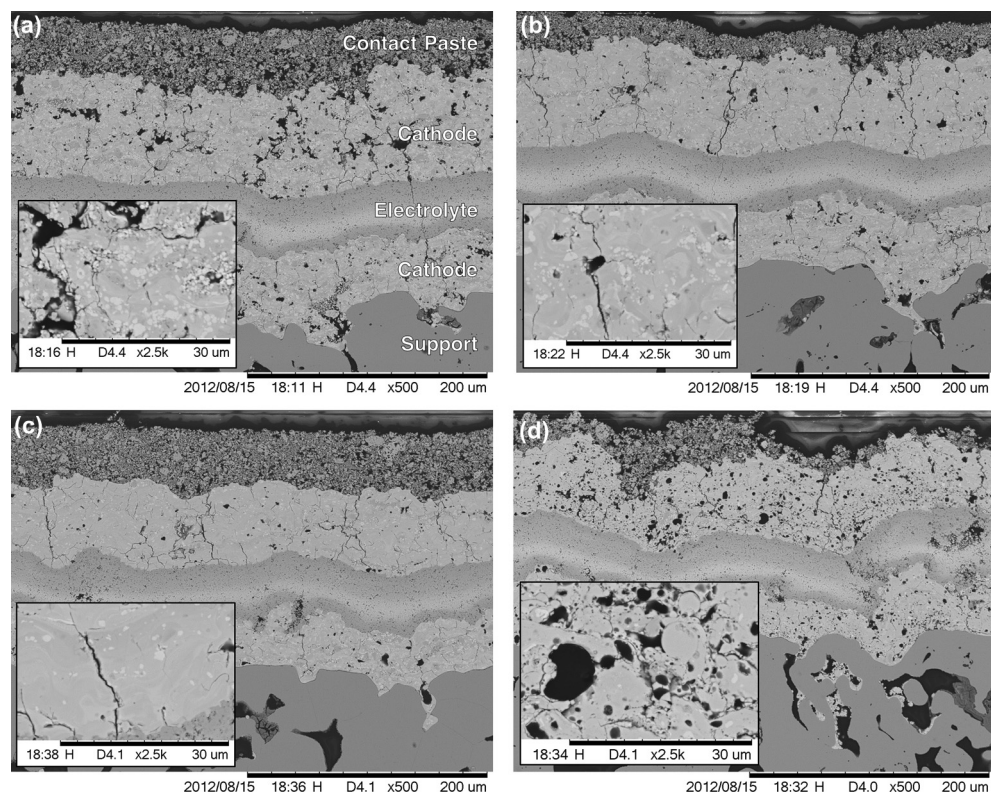


**Fig. 8.** Cross section of metal-supported symmetrical cells containing (a) cathode A, (b) cathode B, (c) cathode C, (d) cathode D.

Backscattered electron micrographs of symmetrical cells A, B, and C are shown in Fig. 8, where the contrast between the two cathode phases is apparent: the SDC phase appears slightly brighter than the LSCF phase. All three cathodes have similar microstructures, with fine regions of SDC well-dispersed within an LSCF matrix, thus explaining the similarities in  $R_p$ . Estimated by image analysis, the cathode porosities were 7%, 4%, and 5% for symmetrical cells A, B, and C, respectively. Of these three cells, the cell A had the highest porosity. Due to this porosity, this cathode likely had more electrochemical reaction sites than cathodes B or C, which may be why cathode A has a lower  $R_p$  than cathode B or C.

### 3.3. Gas transport properties

Ideally, cathodes should have high air permeabilities so that oxygen can easily reach electrochemical reaction sites. Additionally, cathodes with high permeabilities also usually have high porosities (since permeability is proportional to porosity), and therefore, they have a greater reaction surface area where electrochemical reactions can occur. The permeability of cathode A was calculated as  $3.2 \times 10^{-16} \text{ m}^2$ . In an effort to increase this permeability, starch was mixed with the plasma spray feedstock at a starch-to-ceramic mass ratio of 1:3. It has previously been shown that the porosity of a plasma sprayed SOFC electrode can be increased by mixing a sacrificial “pore former” phase with the feedstock [25,26]. During fabrication, the pore former embeds in the electrode and subsequently burns out, creating pores. As listed in Table 3, cathode D was fabricated using the feedstock with 25 wt% pore former and the same process parameters as cathode A. Indeed, the cathode D, made with pore former, had a higher permeability of  $5.0 \times 10^{-16} \text{ m}^2$  and a higher porosity of 12% (compared to 7% for cathode A), shown in Fig. 8(d).

Electrochemical impedance spectroscopy was performed on a symmetrical cell consisting of the more permeable cathodes (cell D), and the Arrhenius plot of the apparent cell  $R_p$  is shown in Fig. 7. In this plot, it appears that the activation energy of cell D significantly decreases as the temperature decreases, and becomes notably non-linear. This behaviour is typical of a symmetrical cell with internal electronic short circuiting. Previously, it has been shown that when there is internal short circuiting, the apparent (or measured)  $R_p$  of a symmetrical cell is lower than the actual cell  $R_p$ ,

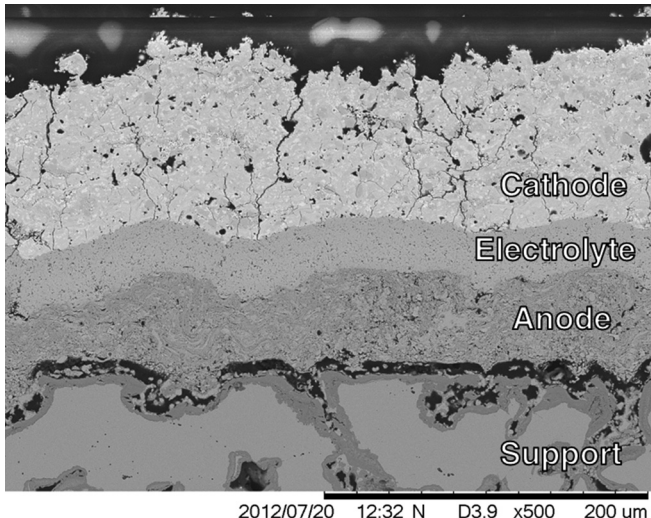


Fig. 9. Cross section of a metal-supported fuel cell with the LSCF and SDC phases finely mixed in the cathode.

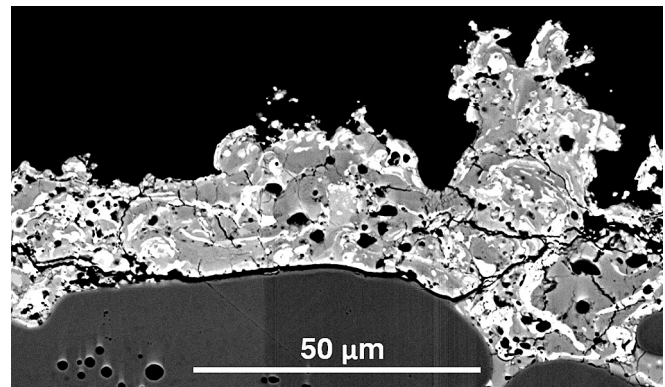


Fig. 10. Cross section of a cathode where the LSCF and SDC phases are coarsely mixed. High contrast is used to distinguish the SDC (bright regions) from the LSCF (darker regions).

and the difference between the apparent and actual  $R_p$ ’s is much greater at lower temperatures than at higher temperatures [27,28].

It is believed that electronic short circuiting occurs as a result of the cathode surface roughness. For cathode D, the average surface roughness ( $R_a$ ) was relatively high,  $12.9 \pm 0.6 \mu\text{m}$ , compared to a roughness of  $7.1 \pm 1.1 \mu\text{m}$  for cathode A, which was made without pore formers. A cathode with such a high surface roughness has deep valleys that need to be “bridged” by the electrolyte. Since plasma spraying is a line-of-sight deposition process, it is difficult to bridge such deep valleys [29]; this can mean that the electrolyte incompletely covers the cathode, thus allowing the two cathodes in

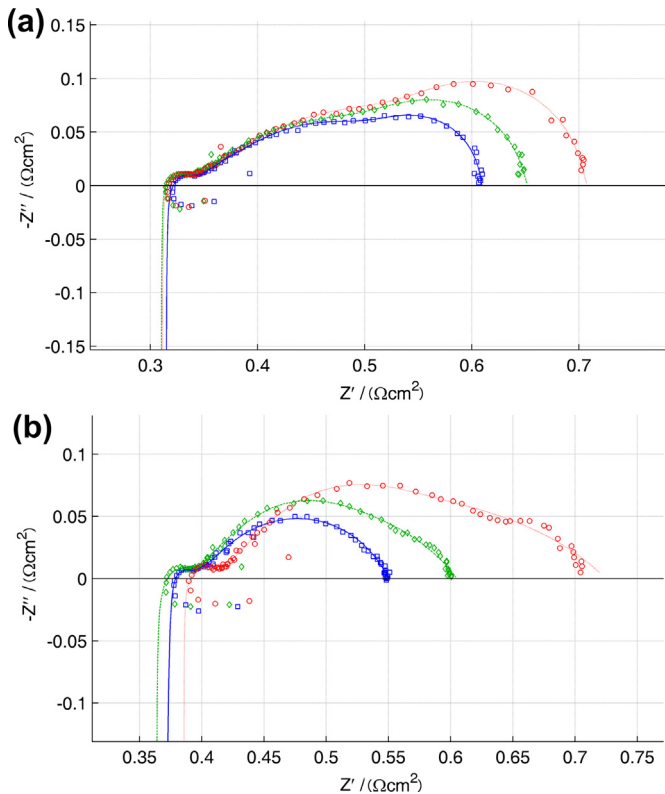
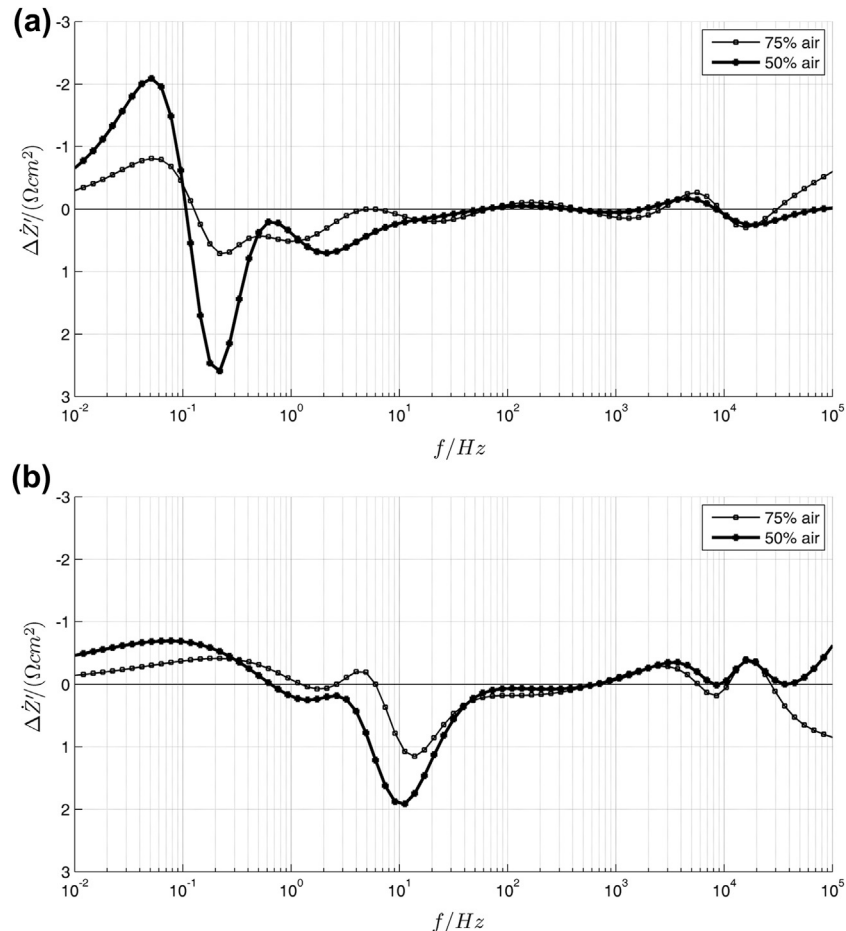


Fig. 11. Electrochemical impedance spectra of fuel cells at 750 °C polarized to 200 mV below the open circuit potential, where the cathode gas consists of 100% air (□), 75% air/25% nitrogen (◇), and 50% air/50% nitrogen (○). Cells contain LSCF–SDC cathodes in which the two phases are (a) finely mixed, and (b) coarsely mixed.



**Fig. 12.** Analysis of differential impedance spectra, where the  $\Delta Z'$  spectra show impedance changes when the cathode gas, initially containing 100% air, is diluted to 75% air and 50% air (balance nitrogen). Spectra are for polarized cells at 750 °C that contain cathodes in which the LSCF and SDC phases are (a) finely mixed, and (b) coarsely mixed.

the symmetrical cell to contact each other [28]. Such contact between the two electrodes causes internal electronic short circuiting.

### 3.4. Fuel cell performance

#### 3.4.1. Cell polarization and power

A metal supported fuel cell was produced, containing the cathode that had the lowest  $R_p$  in a symmetrical cell (cathode A), and a micrograph of the cross section of the fuel cell is shown in Fig. 9. Notably, the LSCF and SDC phases are mixed together finely, as a result of the nano-structured plasma spray feedstock. For comparison, another metal supported fuel cell was fabricated from a heterogeneous feedstock that consisted of a mixture of separate LSCF and SDC particles. The process for plasma spraying the heterogeneous feedstock was previously developed [19], and the LSCF and SDC phases are mixed coarsely in these cathodes, as shown in the micrograph in Fig. 10.

At 750 °C, the open circuit potentials of the fuel cells were 0.899 and 0.917 V, and the peak power densities were 317 and 348 mW cm<sup>-2</sup> for the cells with finely-mixed and coarsely-mixed cathodes, respectively. For both cells, the open circuit potentials were well below the Nernst potential due to gas leakage across the electrolyte. Since the open circuit potentials are different in the two cells, the peak power densities of the two cells cannot be used to meaningfully compare the two different cathodes to each other.

#### 3.4.2. Analysis of impedance

To identify the contributions of the cathode to the cell performance, the cathode gas composition was varied by diluting air with nitrogen: cathodes were tested in 100% air, 75% air, and 50% air atmospheres. In each atmosphere, the electrochemical impedance spectrum was measured at 200 mV below the open circuit potential. An equivalent circuit consisting of 4 RQ elements in series with an inductor ( $L$ ) and ohmic resistor ( $R_S$ ) was fit to the data points in each impedance spectrum, and the polarization resistance was calculated from the equivalent circuit. The analysis of differential impedance spectra (ADIS) method [30] was used to investigate how the cathode contributes to the overall impedance. In the ADIS method, a test parameter (e.g. cathode gas composition) is changed, and the derivative of the real impedance with respect to the natural logarithm of frequency,  $\partial Z'/\partial \ln(f)$ , is measured before and after the test parameter is changed. The difference between the impedance derivatives,  $\Delta Z'$ , is estimated using the formula in Equation (2), where  $Z'_A$  and  $Z'_B$  are the real impedance at conditions A and B, respectively, and  $\omega$  is the angular frequency.

$$\Delta Z' \approx \frac{[Z'_B(\omega_{n+1}) - Z'_B(\omega_{n-1})] - [Z'_A(\omega_{n+1}) - Z'_A(\omega_{n-1})]}{\ln(\omega_{n+1}) - \ln(\omega_{n-1})} \quad (2)$$

The impedance spectra for the cells at 750 °C are shown in Fig. 11. At 750 °C, the polarization resistances of the cells with finely-mixed and coarsely-mixed cathodes were 0.295 and 0.184 Ω cm<sup>2</sup>, respectively. These low  $R_p$  values indicate that oxygen

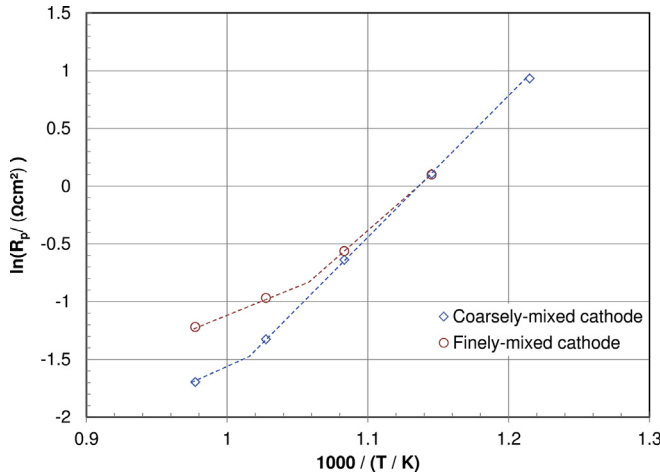


**Fig. 13.** Arrhenius plot of metal supported fuel cells containing LSCF–SDC composite cathodes.

may diffuse well through the cathodes even through the porosity estimates (by image analysis) seem low. One reason for this apparent discrepancy is that thermal spray coatings have a unique microstructure because the solidification of splats results in a lamellar structure. In addition to the larger pores that are visible in Figs. 9 and 10, there is fine porosity between lamellae and fine

cracks perpendicular to the lamellae. Such fine sub-micron porosity can be difficult to quantify using image analysis: the greyscale-value of these features is strongly affected by the large electron generation volume (due to the high accelerating voltages in the SEM).

Dilutions of the cathode gas enlarge the impedance spectra of both cells, as shown in Fig. 11; however, the cell with the coarsely-mixed cathode is more strongly affected than the cell with the finely-mixed cathode. To further analyse these impedances, ADIS plots showing the impedance changes when the cathode gas containing 100% air is diluted to 75% and 50% air (balance nitrogen) are shown in Fig. 12. The ADIS plot for the cell containing the finely-mixed cathode (made from a nano-structured feedstock) has a large low-frequency peak; this suggests that the cathodic impedance is dominated by diffusion. In contrast, the ADIS plot for the cell with the coarsely-mixed cathode has a smaller low-frequency peak, suggesting that diffusion has a lower contribution to the cathodic impedance. In this plot, there are two substantial high-frequency peaks: one is between 1 and 8 kHz, and the other is between 10 and 30 kHz. These are the frequencies at which the impedance is typically affected by charge transfer and transport of oxide ions, respectively [31].

The characteristics of the cathodic impedance are consistent with microstructures of the cathode. The finely-mixed cathode has a low porosity, as shown in Fig. 9, and consequently the impedance is heavily influenced by diffusion. On the other hand, the coarsely-mixed cathode, shown in Fig. 10, has a higher porosity, and the

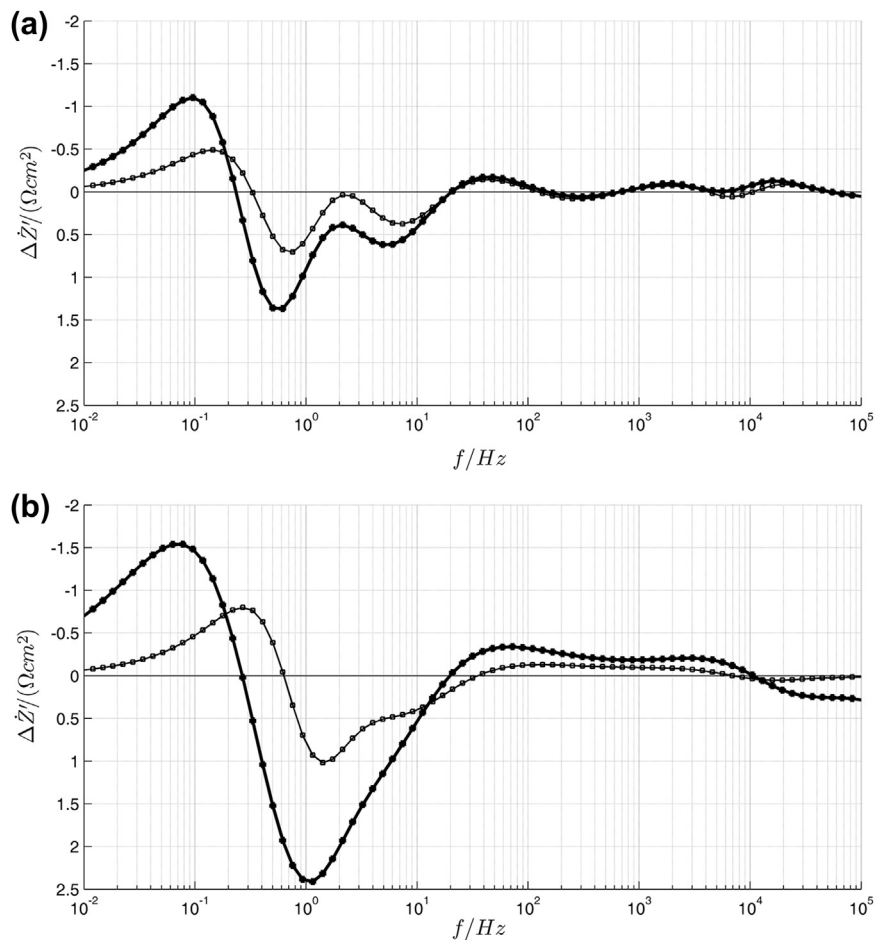


**Fig. 14.** Analysis of differential impedance spectra, where the  $\Delta Z'$  spectra show impedance changes when the cathode gas, initially containing 100% air, is diluted to 75% air and 50% air (balance nitrogen). Spectra are for polarized cells at 650 °C that contain cathodes where the LSCF and SDC phases are (a) finely mixed, and (b) coarsely mixed.

impedance is less influenced by diffusion. Due to the coarse mixing of the LSCF and SDC phases, this cathode has fewer potential reaction sites than the finely-mixed cathode, and thus charge transfer more significantly affects the impedance.

Additionally, the ADIS plot of the coarse cathode has a valley at a frequency of approximately 10 Hz. The magnitude of impedance at this frequency (0.5 Hz–20 Hz) is known to decrease with current passage [31], and therefore this valley is understood as an artifact of cathode activation.

### 3.4.3. Impedance behaviour changes at lower temperatures

Electrochemical impedance spectra were subsequently measured at lower temperatures (polarized at 200 mV below the open circuit potential), and the  $R_p$  values were calculated from equivalent circuit modelling. Arrhenius curves for the polarization resistances for the two cells are plotted in Fig. 13. In both cells, the activation energies change as the operating temperature is lowered, but remain linear, indicating a change in the reaction kinetic mechanism. For the cell with the coarsely-mixed cathode, the activation energy changes between 750 °C and 700 °C, and for the cell with the finely-mixed cathode, the activation energy changes between 700 °C and 650 °C. To investigate the nature of the change in reaction kinetic mechanism, the ADIS plots were obtained for these cells at 650 °C, as shown in Fig. 14. These plots show additional peaks between 10 and 100 Hz that were not present at 750 °C. This frequency band is strongly related to the triple phase boundary (TPB) length in LSM–YSZ cathodes [31]. In LSCF–SDC cathodes, however, the kinetics differ from LSM–YSZ cathodes because LSCF is a mixed conductor, and so the electrochemical reaction zone extends beyond the TPBs [32]. At lower temperatures, however, the ionic conductivity of LSCF decreases, and consequently the electrochemical reaction zone is more confined to the TPB. Therefore, as the cell operating temperature is lowered, a change in reaction kinetics occurs because the TPB length becomes more limiting. The more finely-mixed cathode naturally has a greater TPB density than the coarsely-mixed cathode, and therefore the change in reaction mechanism occurs at a lower temperature.

## 4. Summary

A plasma spray process was developed for fabricating composite LSCF–SDC cathodes from a nano-structured powder feedstock. In these cathodes, the LSCF and SDC phases were mixed together very finely so that there were a large number of potential reaction sites, but the low porosity limited the number of reaction sites. The effects of process parameters were assessed by SEM and XRD, and electrochemical impedance spectroscopy was performed on symmetrical cells to evaluate cathodes made with the most promising sets of process parameters.

A composite LSCF–SDC cathode was incorporated into a metal supported fuel cell with a nickel–YSZ anode and YSZ electrolyte. The effect of the cathode microstructure on the cell impedance was investigated through the analysis of differential impedance spectra (ADIS). At higher temperatures (750 °C), the cathode impedance is dominated by diffusion when the LSCF and SDC phases are finely

mixed. In contrast, when the LSCF and SDC phases are coarsely mixed, charge transfer kinetics have a greater impact on the impedance, because there are fewer potential reaction sites. At lower operating temperatures (650 °C), the cell impedances are more strongly affected by the TPB density, as the ionic conductivity of LSCF is lower.

## Acknowledgements

The authors gratefully acknowledge financial support from the Natural Sciences and Engineering Research Council of Canada (NSERC) and the SOFC Strategic Research Network. The fuel cell gasket material was generously donated by Flexitallic LP. Additionally, the authors acknowledge the Centre for Advanced Coatings Technology at the University of Toronto for the use of their facilities.

## References

- [1] E.P. Murray, M.J. Server, S.A. Barnett, Solid State Ionics 148 (2002) 27–34.
- [2] F. Tietz, V.A.C. Haanappel, A. Mai, J. Mertens, D. Stöver, J. Power Sources 156 (2006) 20–22.
- [3] W.G. Wang, M. Mogensen, Solid State Ionics 176 (2005) 457–462.
- [4] C. Fu, K. Sun, N. Zhang, X. Chen, D. Zhou, Electrochim. Acta 52 (2007) 4589–4594.
- [5] Y. Leng, S.H. Chan, Q. Liu, Int. J. Hydrogen Energy 33 (2008) 3808–3817.
- [6] G. Schiller, R. Henne, M. Lang, R. Ruckdäschel, S. Schaper, Fuel Cells Bull. 3 (2000) 7–12.
- [7] G. Schiller, R. Henne, M. Lang, M. Müller, Mater. Sci. Forum 426–432 (2003) 2539–2544.
- [8] R. Vaßen, D. Hathiramani, J. Mertens, V.A.C. Haanappel, I.C. Vinke, Surf. Coat. Technol. 202 (2007) 499–508.
- [9] O. Marchand, P. Bertrand, J. Mougin, C. Comminges, M.-P. Planche, G. Bertrand, Surf. Coat. Technol. 205 (2010) 993–998.
- [10] K. Wittmann-Ténèze, A.-L. Sauvet, ECS Trans. 25 (2009) 2319–2326.
- [11] A.A. Syed, Z. İlhan, G. Schiller, in: Thermal Spray 2008: Proceedings from the International Thermal Spray Conference, 2008, pp. 190–194.
- [12] J. Lagerbom, A.-P. Nikkilä, M. Kylmälähti, P. Vuoristo, U. Kanerva, T. Varis, in: Thermal Spray 2008: Proceedings from the International Thermal Spray Conference, 2008, pp. 1103–1108.
- [13] A. Ansar, D. Soysal, Z. İlhan, N. Wagner, S. Wolf, R. Ruckdäschel, ECS Trans. 25 (2009) 2443–2453.
- [14] G. Schiller, A. Ansar, M. Lang, O. Patz, J. Appl. Electrochem. 39 (2009) 293–301.
- [15] J. Harris, O. Kesler, J. Therm. Spray Technol. 19 (2010) 328–335.
- [16] A. Ansar, D. Soysal, Z. İlhan, N. Wagner, in: Thermal Spray 2010: Proceedings of the International Thermal Spray Conference, 2010, pp. 123–128.
- [17] J. Harris, O. Kesler, ECS Trans. 25 (2009) 2455–2461.
- [18] J. Harris, O. Kesler, ECS Trans. 35 (2011) 1927–1934.
- [19] J. Harris, M. Qureshi, O. Kesler, J. Therm. Spray Technol. 21 (2012) 461–468.
- [20] D. Waldbillig, O. Kesler, Surf. Coat. Technol. 205 (2011) 5483–5492.
- [21] D. Waldbillig, O. Kesler, J. Power Sources 196 (2011) 5423–5431.
- [22] C. Metcalfe, J. Harris, J. Kuhn, M. Marr, O. Kesler, J. Therm. Spray Technol. in press
- [23] S. Park, S. Kumar, H. Na, C. Lee, J. Therm. Spray Technol. (2008) 1–7.
- [24] B.D. White, O. Kesler, Adv. Mat. Res. 15–17 (2007) 299–304.
- [25] L.-W. Tai, P.A. Lessing, J. Am. Ceram. Soc. 74 (1991) 501–504.
- [26] M. Poon, O. Kesler, J. Power Sources 210 (2012) 204–217.
- [27] X. Zhang, M. Robertson, C. Deées-Petit, W. Qu, O. Kesler, R. Maric, D. Ghosh, J. Power Sources 164 (2007) 668–677.
- [28] B.D. White, O. Kesler, J. Power Sources 177 (2008) 104–110.
- [29] D. Waldbillig, Z. Tang, A. Burgess, O. Kesler, in: Thermal Spray 2008: Proceedings of the International Thermal Spray Conference (2008), pp. 201–206.
- [30] S.H. Jensen, A. Hauch, P.V. Hendriksen, M. Mogensen, N. Bonanos, T. Jacobsen, J. Electrochem. Soc. 154 (2007) B1325–B1330.
- [31] M.J. Jørgensen, M. Mogensen, J. Electrochem. Soc. 148 (2001) A433–A442.
- [32] S.B. Adler, J.A. Lane, B.C.H. Steele, J. Electrochem. Soc. 143 (1996) 3554–3564.